Asian Journal of Water, Environment and Pollution, Vol. 20, No. 6 (2023), pp. 77-85.
DOI 10.3233/AJW230082

Utilisation of Clamshell Waste for Removing Mercury From Water: Fixed Bed Adsorption and Modelling Studies

S. Baskar*, K.R. Aswin Sidhaarth and L. Mangaleshwaran[1]

Department of Civil Engineering, Vel Tech Rangarajan Dr. Sagunthala R&D Institute of Science and Technology, Chennai, Tamil Nadu, India

[1]Department of Civil Engineering, Alagappa Chettiar Government College of Engineering and Technology, Karaikudi, Tamil Nadu, India

✉ rhodabaskar@gmail.com

Received September 26, 2022; revised and accepted August 4, 2023

Abstract: The present communication investigated the sustainable utilization of the clamshell waste powder (CSP) for eliminating mercury through fixed bed adsorption. This CSP is freshly prepared and packed in a stable multi-port column. Their breakthrough performance in the column is evaluated by varying its bed depth (5, 10, 15, 20 and 25 min) and flow rate (8, 10 and 12 mL/min). The CSP column's design parameters and kinetic behavior are estimated from its breakthrough curve and validated using column models. The results revealed that slow saturation of the CSP bed and maximum adsorption capacity (2.8 mg/g) occurred at lower column depth (5 cm) and elevated influent flow rates (12 mL/min). Moreover, the mass transfer zone exhibited fluctuations with elevated column depth, indicating the presence of non-ideal conditions. The YN model showed superior fitness for mercury removal using CSP. The dynamic studies showed that CSP is a cost-effective, eco-friendly, biocompatible and sustainable adsorbent that can be successfully employed for treating industrial effluent.

Key words: Adsorption, clam shell, dynamic modelling, fixed bed column, mercury removal.

Introduction

Maintaining sustainability in the aqueous environment has become a global concern. The main factor was the continuous release of treated or moderately treated wastewater into the aqueous bodies, which had a greater environmental impact. Many stringent rules have been implemented by the government to eradicate the problem of water resources getting polluted. Heavy metal abatement has attracted major attention in recent decades due to its toxicity level (Jayaswal et al., 2018). Mercury (Hg) is one of such heavy metals (maximum permissible limit: 0.006 mg/L) that tend to bioaccumulate in living organisms and get biomagnified (Ghasemi et al., 2019; Suresh et al., 2019). It causes health issues like lung cancer, nasal tumour, sinus, nervous system damage, etc. (Sumesh et al., 2011). Therefore, their elimination has become a vital need in society. Many treatment technologies have been in practice for their eradication, such as adsorption (Naushad et al., 2019), electrocoagulation (De et al., 2019), membrane filtration (Urgun-Demirtas et al., 2012) and photocatalytic degradation (Tsai et al., 2019). Adsorption still has some advantages over other advanced technologies due to the following reasons: Simple and economical operation, less labour and land

*Corresponding Author

requirement, no generation of secondary pollutants, highly efficient, etc. (Jayalakshmi & Jeyanthi, 2019; Rangabhashiyam et al., 2013).

Clams (*Mercenaria mercenaria*) are shellfish capable of growing rapidly within a shorter breeding cycle found in coastal lagoons, lakes and estuaries. However, their shell is the by-product of aquaculture, primarily discarded along with its remnant. Therefore, it is not beneficially utilised and it adds a burden to the environment as a bio-waste. Moreover, it may potentially produce toxins when exposed to the environment for a longer time (Qu et al., 2022). The clamshell is mainly composed of calcium carbonate ($CaCO_3$) and chitin, which has a high affinity toward toxic heavy metals (Murphy et al., 2017). Due to this fact, their utilisation as an adsorbent has fascinated many researchers. Up to date, either carbonized or functionally modified clamshells have been reported to remove various pollutants, including toxic heavy metals and dyes (El Haddad et al., 2014; Núñez et al., 2019; Papadimitriou et al., 2017).

In this study, the powdered clamshell with no carbonisation and functional modification is utilised in dynamic adsorption for Hg removal. Hence, the utilisation of harmful chemicals is avoided, and the preparation of CSP does not require the use of highly complex gear or skilled labour. Their preparation method requires the use of milling machines, with the expenses being dependent only on the electricity costs associated with it. The reutilisation of CSP as an adsorbent serves to minimise waste accumulation, as they are considered biowaste material.

In the present study, the CSP is compactly packed in a multi-port fixed bed column. Its competency in the dynamic flow process is evaluated to determine its equilibrium attainment. The CSP is characterised using XRD, SEM and TEM analysis to identify its physical nature. An assessment was conducted to determine the CSP column depth and influent flow rate's impact on the Hg removal, hence determining the design parameters of the column. The kinetic behaviour of CSP in the fixed bed column was validated with the YN and Th models.

Methodology

Chemicals Used

Mercury (II) chloride ($HgCl_2$), sodium hydroxide (NaOH) and hydrochloric acid (HCl) were procured from Merck (analytical grade). Deionised water was utilised for preparing the reagents.

Preparation of Clamshell powder

The preparation of clamshell powder is elaborated in Figure 1.

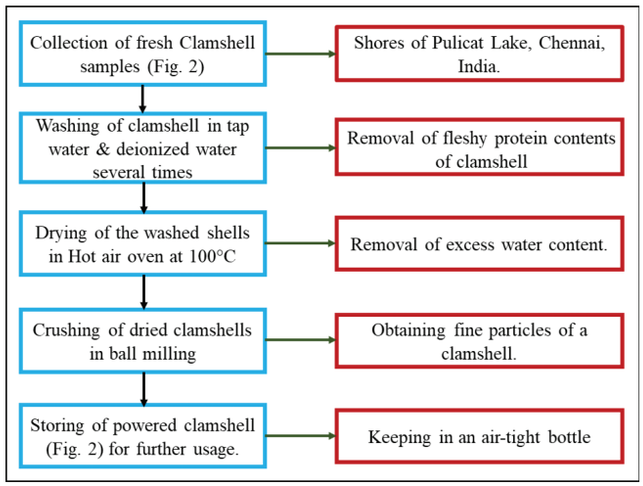

Figure 1: Preparation of clamshell powder.

Characterisation of Clamshell Powder

The clamshell powder was analysed using XRD (Empyrean, Malvern PANalytical), SEM (JEOL JSM-7600F) and TEM (PHILIPS CM 200) analysis. The XRD analysis determined the CSP's phase formation, whereas their surface morphology was visualised from SEM and TEM analysis. The XRD pattern was generated at 40 kV over the 2θ range of 10º-80º using a Cu target with a wavelength of 1.54 Å. The SEM was operated under the accelerating voltage of 10 kV and magnification up to 75,000×. The TEM was operated under the voltage of 20–200 kV with a resolution of 2.4 Å.

Fixed-Bed Column Packed with Clamshell Powder

A stable multi-port column made of glass was used to perform continuous removal of mercury and their operating procedure were illustrated in Figures 2 and 3, respectively..

Mathematical Analysis of Breakthrough Curve

The breakthrough curve was analysed to evaluate the performance and design parameters of the column for Hg adsorption using CSP. The graph plotted with C_t/C_0 versus time frames the breakthrough curve of the fixed-bed column (Babazadeh et al., 2021; Jayalakshmi et al., 2021). Moreover, the parameters obtained from such a curve describe the CSP bed's adsorption approach for Hg removal. The design parameters are calculated to assess the dynamic behaviour of CSP.

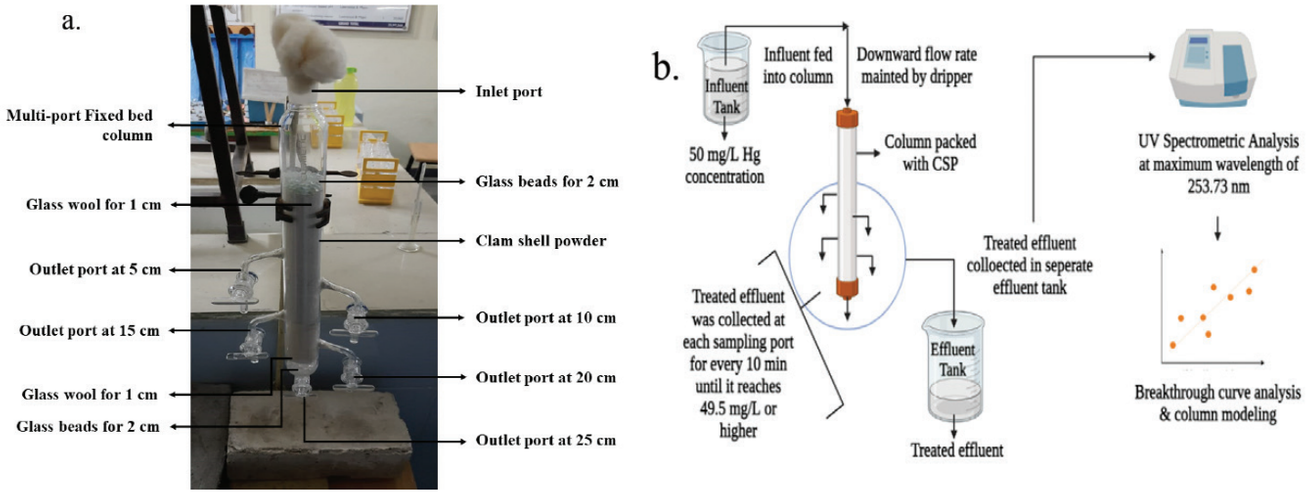

Figure 2: (a) Experimental fixed bed column and (b) operating protocol for dynamic adsorption of Hg using CSP.

Dynamic Modeling and Error Analysis

The effectiveness of the CSP column bed for mercury uptake was validated using dynamic modeling - YN and Th model (Sugashini et al., 2014). Moreover, their corresponding parameters were obtained by plotting a non-linear regression graph of C_t/C_0 vs. t. The non-linear form of YN and Th was presented in eqs. (1) and (2), respectively (Idan et al., 2017).

$$\frac{C_t}{C_O} = \frac{1}{1+e^{\kappa_{YN}(\tau - t)}} \tag{1}$$

$$\frac{C_t}{C_O} = \frac{1}{1+\exp\left(\frac{\kappa_{Th}}{Q}(q_e m - C_o t)\right)} \tag{2}$$

The appropriateness of the non-linear regression approach for dynamic modeling is validated using error analysis techniques (Jayalakshmi & Jeyanthi, 2019), which are as presented below.

$$R^2 = 1 - \frac{\sum_{n=1}^{n}(y_{e(n)} - y_{c(n)})^2}{\sum_{n=1}^{n}(y_{e(n)} - y_{e(mean)})^2} \tag{3}$$

$$\text{RMSE} = \sqrt{\frac{1}{n-1}\sum_{n=1}^{n}(y_{e(n)} - y_{c(n)})^2} \tag{4}$$

$$\text{SSE} = \sum_{i=1}^{n}(y_c - y_e)_i^2 \tag{5}$$

$$X^2 = \sum_{n=1}^{n}\frac{(y_{e(n)} - y_{c(n)})^2}{y_{e(n)}} \tag{6}$$

Results and Discussion

Structural and Morphological Description of Clamp Shell Powder

The diffraction pattern of the CSP reveals the presence of calcium carbonate (aragonite $CaCO_3$). This is confirmed by the existence of planar indices (111), (121), (102), (220), (202) and (113) (JCPDS card No. 00-001-1033) (Asikin-Mijan et al., 2015). Further, the crystallite size of the CSP is calculated using the Debye–Scherrer formula (Santhosh & Prabu, 2012), which is represented in eq. (7) and it was found to be 66 nm.

$$d_{XRD} = \frac{0.9\lambda}{\beta\cos\theta} \tag{7}$$

$V_{eff} = Qt_{total}$	Volume of effluent collected
$q_{total} = \frac{QA_c}{1000} = \frac{Q}{1000}\int_{t=0}^{t=t_{total}} C_{ads}dt$	Maximum bed capacity
$q_{0,exp} = \frac{q_{total}}{m}$	Maximum adsorption capacity at exhaustion time
$M_{total} = \frac{C_0 Qt_{total}}{1000}$	Total amount of mercury ions that entered the column
$EBRT = \frac{\text{Volume of CSP bed}}{\text{volumetric flow rate of Mercury solution}}$	Empty Bed Resistance Time (EBRT)
$TR\ (\%) = \frac{q_{total}}{M_{total}} \times 100$	Total mercury removal (TR)
$MTZ = H\left(1 - \frac{t_b}{t_{total}}\right)$	Mass Transfer Zone (MTZ)
$\Delta t = t_e - t_b$	Overall adsorption zone
$r_f = \frac{V_{50\%}}{AH\varepsilon}$	Retardation factor

Figure 3: Design parameters for CSP's column.

The morphological characteristics such as texture, geometric structure and shape of the clamshell powder are examined using an SEM (Figure 4a-b) and TEM (Figure 4c) analysis. As a result, the morphology of the CSP revealed its geometric structure to be irregularly shaped, particle distribution to be non-uniform and the particles are found to be agglomerated. Furthermore, their CSP particle distribution was 40–90 nm.

Analysis of Design Parameters of CSP Column

The effectiveness of CSP in a fixed-bed column for removing mercury is assessed at varied bed depths (5-25 cm). Also, it is determined at varied flow rates of 8–12 mL/min. Figure 5 presents the breakthrough curves for mercury adsorption using CSP at a varied rate of influent flow. These breakthrough curves for Hg adsorption showed a typical characteristic S-shaped curve where their variations depended on CSP dosage and flow rate. The design parameters calculated from the respective breakthrough curves (Singh et al., 2017) are presented in Table 1. The obtained parameters exhibited inclined values for higher column depth and a slow movement of mercury ions.

It was noted that the contact time between the CSP and Hg ions may increase due to the higher loading of CSP in maximum bed height (Chowdhury & Saha, 2013). Consequently, a prominent inclination was observed in the values of breakthrough time as well as exhaustion time (Table 1). Moreover, the higher t_b resulted in a rise in the capacity of the CSP bed. An

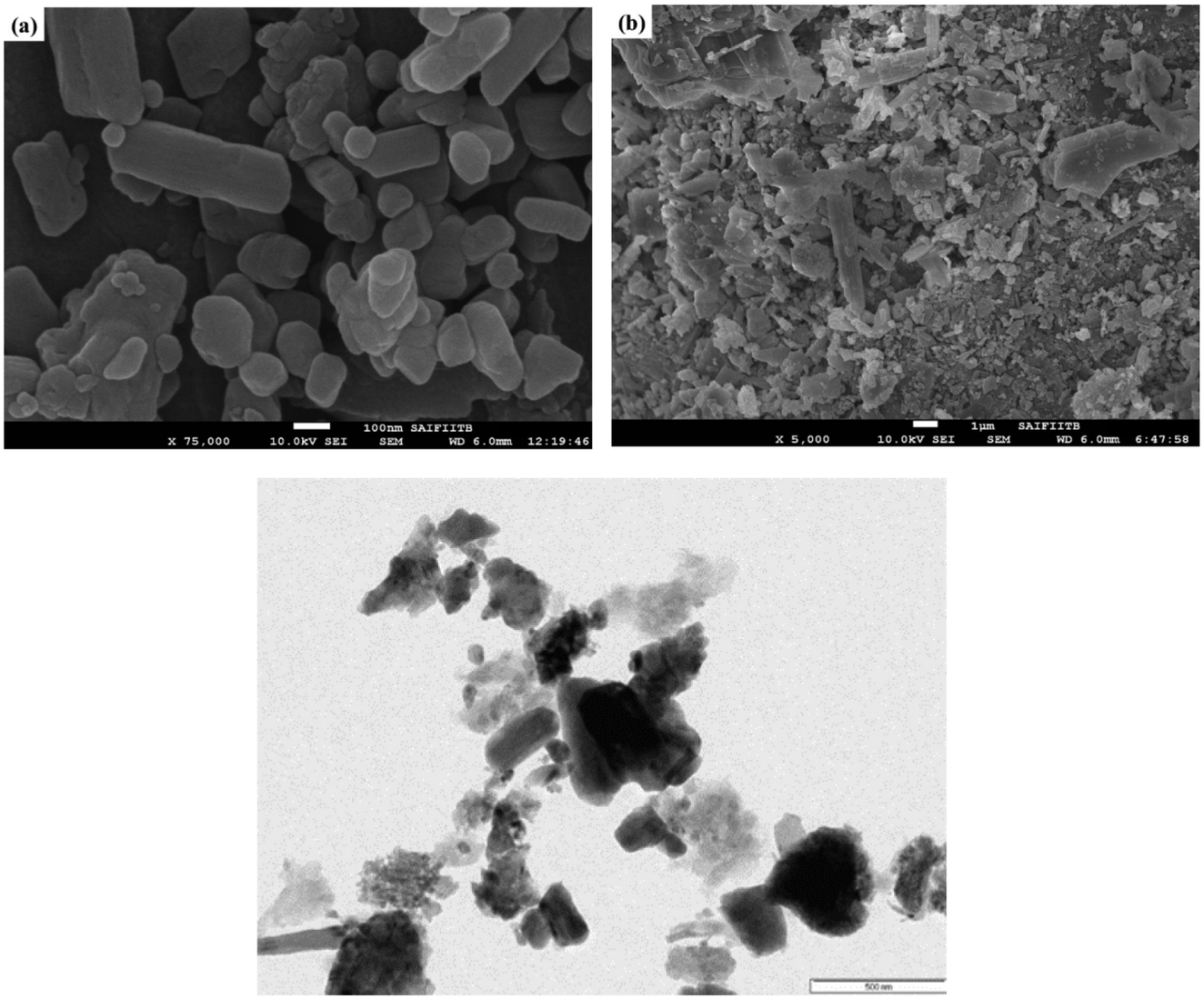

Figure 4: SEM micrograph of clamshell powder under magnification (a) ×75,000, (b) ×5000 and (c) TEM image of clamshell powder (scale bar 500 nm).

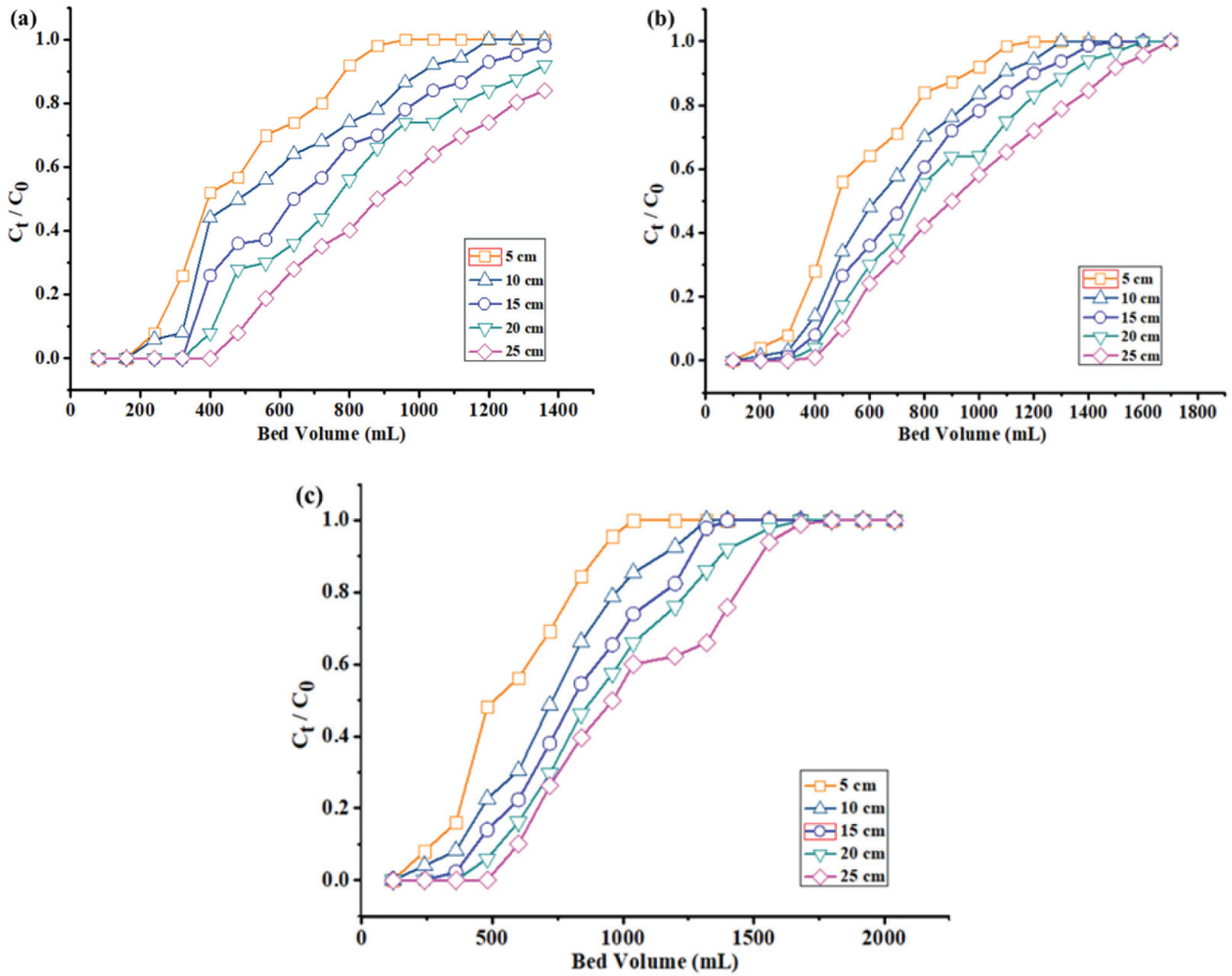

Figure 5: (a) CSP column's breakthrough curve for mercury adsorption at Flow rate - 8 mL/min, (b) at Flow rate - 10 mL/min and (c) at Flow rate - 12 mL/min.

increase in the exposure of the mercury ions with CSP may be attributed to the rise in removal percentage. Furthermore, the values of V_{eff} increased, which may be due to the rise in residence time within the CSP bed (Amiri et al., 2017).

The values of Δt, r_F and MTZ depend on the residence time changes. The increase in column depth results in increased residence time and vice versa. Therefore, the values of Δt and the MTZ showed an inclined trend with the rise in the time available for mercury ions to contact the CSP (Hernandez-Eudave et al., 2016). Meanwhile, r_F values exhibited a declining trend with increased CSP column depths (Mishra et al., 2016). The greater utilization of the CSP column has occurred at a maximum bed depth of 25 cm (Nithya et al., 2020).

On the contrary, the effect of flow rate showed a different trend on the design parameters (Table 1). The increase in the flow rate resulted in increased velocity, thereby increasing the mass transfer rate (Gong et al., 2021). As a result, the values of t_b and t_e get reduced. Conversely, the increased mass transfer rate is attributed to the higher uptake of Hg ions, which is evident from the rise in q_{total} values (Table 1). As the flow rate increases, the movement of mercury ions passing through the CSP bed increases, resulting in faster bed saturation. Due to this, V_{eff} values may decrease, leading to lowered adsorption zone (Δt) and decreased removal percentage. The faster saturation of the CSP bed also resulted in a decreased mass transfer zone (MTZ) (Table 1) (Qu et al., 2019). Moreover, the elevated flow rate showed an inclined pattern of r_F values

which may be due to the higher residence time (Nithya et al., 2021). Therefore, the optimal usage of the CSP bed was attained at 8 mL/min influent flow.

Assessment of YN and Th Model Parameter on the Mercury Uptake

The breakthrough data obtained from column data were further assessed using the YN and Th models. Their corresponding parameters, as well as their error analysis values, are given in Tables 2 and 3.

For both the models, the R^2 values ranged from 0.9796 to 0.9359 and the values of RMSE, χ^2 and SSE seem to be lower, indicating their best fitness. However, the YN model showed closer values of $q_{e(\mathrm{cal})}$ and $q_{e(\mathrm{exp})}$

Table 1: Evaluation of design parameters of CSP column

Influent Flow rate mL/min	*Bed depth cm*	*EBRT min*	t_b *min*	t_{total} *min*	Δt *min*	r_f	V_{eff} *mL*	M_{total} *mg*	q_{total} *mg*	*MTZ cm*	*Percent Removal %*
8	5	12	35	100	84	0.849	800	40	19.69	3.3	49.22
	10	25	40	130	111	0.339	1040	52	25.07	6.9	48.21
	15	37	45	150	119	0.226	1200	60	30.71	10.5	51.19
	20	49	50	168	120	0.153	1344	67.2	35.05	14.0	52.15
	25	61	62	170	135	0.124	1360	68	40.61	15.9	59.72
10	5	10	32	100	78	1.061	1000	50	22.79	3.4	45.59
	10	20	38	110	90	0.424	1100	55	28.71	6.5	52.20
	15	29	40	120	97	0.265	1200	60	32.71	10.0	54.52
	20	39	45	125	101	0.169	1250	62.5	36.93	12.8	59.09
	25	49	50	140	115	0.127	1400	70	42.07	16.1	60.1
12	5	8	25	75	65	1.273	900	45	22.21	3.3	49.36
	10	16	32	100	84	0.509	1200	60	30.57	6.8	50.95
	15	25	40	105	85	0.297	1260	63	35.88	9.3	56.96
	20	33	45	110	89	0.191	1320	66	40.54	11.8	61.42
	25	41	50	120	90	0.144	1440	72	46.01	14.6	63.90

Table 2: YN model parameters for mercury adsorption onto the CSP

Flow rate mL/min	*h cm*	*Yoon-Nelson model Parameter*				*Error Analysis*			
		τ *min*	K_{YN} *L/min*	$q_{e\,(cal)}$ *mg/g*	$q_{e\,(exp)}$ *mg/g*	R^2	*RMSE*	χ^2	*SSE*
8	5	57.09	0.0620	1.92	1.97	0.9796	0.0556	0.2377	0.0262
	10	69.56	0.0446	1.20	1.25	0.9591	0.0765	0.4182	0.0565
	15	84.50	0.0412	0.98	1.02	0.9737	0.0608	0.4102	0.0573
	20	96.75	0.0384	0.84	0.88	0.9777	0.0532	0.3403	0.0775
	25	114.08	0.0353	0.79	0.81	0.9799	0.0461	0.3199	0.0639
10	5	57.09	0.0620	2.25	2.28	0.9764	0.0591	0.2127	0.0415
	10	69.56	0.0446	1.41	1.44	0.9748	0.0665	0.3190	0.0819
	15	84.50	0.0412	1.02	1.09	0.9419	0.0975	0.4632	0.8696
	20	96.75	0.0384	0.89	0.92	0.9359	0.1160	0.6407	1.4922
	25	92.81	0.0420	0.81	0.84	0.9880	0.0451	0.2660	0.0286
12	5	46.53	0.0803	2.20	2.22	0.9889	0.0391	0.1077	0.0008
	10	61.00	0.0698	1.50	1.53	0.9977	0.0191	0.0466	$1.91\text{x}10^{-05}$
	15	69.43	0.0643	1.18	1.20	0.9937	0.0330	0.1131	0.00068
	20	76.53	0.0595	0.99	1.01	0.9941	0.0320	0.1452	0.0092
	25	85.60	0.0488	0.89	0.92	0.9760	0.0634	0.3135	0.01005

Table 3: Th model parameters for mercury adsorption onto the CSP

Flow rate mL/min	*h cm*	*Thomas model Parameter*			*Error Analysis*			
		K_{Th} *L/min*	$q_{e\ (cal)}$ *mg/g*	$q_{e\ (exp)}$ *mg/g*	R^2	*RMSE*	χ^2	*SSE*
8	5	0.0012	2.28	1.97	0.9796	0.0556	0.2377	0.0262
	10	0.0008	1.39	1.25	0.9591	0.0765	0.4182	0.0565
	15	0.00082	1.12	1.02	0.9737	0.0608	0.4102	0.0573
	20	0.00076	0.96	0.88	0.9777	0.0532	0.3403	0.0775
	25	0.00070	0.91	0.81	0.9799	0.0461	0.3199	0.0639
10	5	0.00140	2.66	2.28	0.9846	0.0478	0.1564	0.0367
	10	0.00117	1.64	1.44	0.9905	0.0407	0.1695	0.0235
	15	0.00110	1.22	1.09	0.9917	0.0367	0.1853	0.0242
	20	0.00096	1.02	0.92	0.9857	0.0475	0.2402	0.0321
	25	0.00084	0.92	0.84	0.9857	0.0451	0.2660	0.0286
12	5	0.00161	2.80	2.22	0.9889	0.0391	0.1076	0.0008
	10	0.00139	1.82	1.53	0.9977	0.0191	0.0466	1.91×10^{-5}
	15	0.00128	1.38	1.20	0.9937	0.0330	0.1131	0.00068
	20	0.00119	1.14	1.01	0.9941	0.0320	0.1452	0.0092
	25	0.00097	1.02	0.92	0.9760	0.0634	0.3135	0.01005

when compared to the Th model (Hassan & Hrdina, 2018). Therefore, the YN model results substantiate its better fitness for mercury adsorption onto CSP.

The values of τ (Table 2) exhibited an inclined trend with elevated CSP bed attributing to the maximum availability of adsorption sites. The rapid saturation of the CSP bed occurs at elevated flow rates, which may be attributed to the decreased values of τ (Jayalakshmi et al., 2022). The adsorption rate (K_{YN}) values decreased with increasing CSP column depth and lowering flow rate.

The Thomas rate constant (K_{Th}) (Table 3) exhibited decreasing values with higher CSP column depth as a result of reduced mass transfer rate (Das et al., 2021). Therefore, the reduced mass transfer rate with higher bed depth may be attributed to the decreased values of K_{Th} (Vishalia et al., 2019). Similarly, the maximum q_e is achieved with lower CSP bed depth and higher flow rate.

Feasibility of CSP Adsorbent

The CSP adsorbent was observed to satisfy the feasibility criteria for more extended-run applications, which are represented in Figure 6.

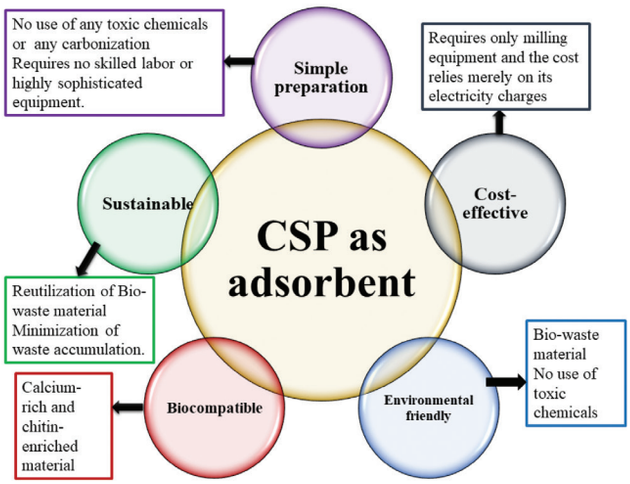

Figure 6: Feasibility of CSP adsorbent.

Conclusion

The simultaneous approach of clamshell waste utilization and mercury elimination in a CSP column demonstrated an effective mercury removal with a maximum bed capacity of 46.01 mg. Design parameters that are estimated from the CSP column performance showed that it is highly bed depth-dependent. Moreover, a low flow rate (8 mg/L) and higher column depth (25 cm) resulted in delayed breakthrough, increased mercury uptake and maximum percent removal. Consequently, these factors contribute to the best operating condition for effectively utilising CSP in a fixed bed column for mercury removal. Additionally, these operational strategies have prolonged adsorption cycles, resulting in a reduced frequency of transitioning from adsorption to

regeneration. Furthermore, the CSP column data showed better fitness with the YN model. Thus, CSP showed effective mercury removal that can be utilized as an alternative adsorbent for treating industrial effluents.

References

Amiri, M.J., Abedi-Koupai, J. and S. Eslamian (2017). Adsorption of Hg (II) and Pb (II) ions by nanoscale zero valent iron supported on ostrich bone ash in a fixed-bed column system. *Water Science and Technology*, **76(3):** 671-682.

Asikin-Mijan, N., Taufiq-Yap, Y.H. and H.V. Lee (2015). Synthesis of clamshell derived $Ca(OH)_2$ nano-particles via simple surfactant-hydration treatment. *Chemical Engineering Journal*, **262:** 1043-1051.

Babazadeh, M., Abolghasemi, H., Esmaeili, M., Ehsani, A. and A. Badiei (2021). Comprehensive batch and continuous methyl orange removal studies using surfactant modified chitosan-clinoptilolite composite. *Separation and Purification Technology*, **267:** 118601.

Chowdhury, S. and P. Saha (2013). Artificial neural network (ANN) modeling of adsorption of methylene blue by NaOH modified rice husk in a fixed-bed column system. *Environmental Science and Pollution Research*, **20(2):** 1050-1058.

Das, L., Sengupta, S., Das, P., Bhowal, A. and C. Bhattacharjee (2021). Experimental and numerical modeling on dye adsorption using pyrolyzed mesoporous biochar in batch and fixed-bed column reactor: Isotherm, thermodynamics, mass transfer, kinetic analysis. *Surfaces and Interfaces*, **23:** 100985.

De, S., Hazra, T. and A. Dutta (2019). Assessment of removal of mercury from landfill leachate by electrocoagulation. *In:* Kundu, R., Narula, R., Paul, R. and S. Mukherjee (eds.). Environmental Biotechnology For Soil and Wastewater Implications on Ecosystems. Springer, Singapore. pp. 21-27. https://doi.org/10.1007/978-981-13-6846-2_4

El Haddad, M., Regti, A., Laamari, M.R., Slimani, R., Mamouni, R., El Antri, S. and S. Lazar (2014). Calcined mussel shells as a new and eco-friendly biosorbent to remove textile dyes from aqueous solutions. *Journal of the Taiwan Institute of Chemical Engineers*, **45(2):** 533-540.

Ghasemi, S.S., Hadavifar, M., Maleki, B. and E. Mohammadnia (2019). Adsorption of mercury ions from synthetic aqueous solution using polydopamine decorated SWCNTs. *Journal of Water Process Engineering*, **32:** 100965.

Gong, L., Kong, Y., Wu, H., Ge, Y. and Z. Li (2021). Sodium alginate microspheres interspersed with modified lignin and bentonite (SA/ML-BT) as a green and highly effective adsorbent for batch and fixed-bed column adsorption of Hg (II). *Journal of Inorganic and Organometallic Polymers and Materials*, **31(2):** 659-673.

Hassan, A.F. and R. Hrdina (2018). Chitosan/nanohydroxyapatite composite based scallop shells as an efficient adsorbent for mercuric ions: Static and dynamic adsorption studies. *International Journal of Biological Macromolecules*, **109:** 507-516.

Hernandez-Eudave, M.T., Bonilla-Petriciolet, A., Moreno-Virgen, M.R., Rojas-Mayorga, C.K. and R. Tovar-Gómez (2016). Design analysis of fixed-bed synergic adsorption of heavy metals and acid blue 25 on activated carbon. *Desalination and Water Treatment*, **57(21):** 9824-9836.

Idan, I.J., Abdullah, L., Jamil, S., Obaid, M. and T. Choong (2017). Fixed-bed system for adsorption of anionic acid dyes from binary solution onto quaternized kenaf core fiber. *BioResources*, **12(4):** 8870-8885.

Jayalakshmi, R. and J. Jeyanthi (2019). Simultaneous removal of binary dye from textile effluent using cobalt ferrite-alginate nanocomposite: Performance and mechanism. *Microchemical Journal*, **145:** 791-800.

Jayalakshmi, R. and J. Jeyanthi (2021). Dynamic modelling of alginate-cobalt ferrite nanocomposite for removal of binary dyes from textile effluent. *Journal of Environmental Chemical Engineering*, **9(1):** 104924.

Jayalakshmi, R., Jeyanthi, J. and K.A. Sidhaarth (2022). Versatile application of cobalt ferrite nanoparticles for the removal of heavy metals and dyes from aqueous solution. *Environmental Nanotechnology, Monitoring & Management*, **17:** 100659.

Jayaswal, K., Sahu, V. and B.R. Gurjar (2018). Water pollution, human health and remediation. *In:* Bhattacharya, S., Gupta, A., Gupta, A. and A. Pandey (eds.). Water Remediation. Energy, Environment, and Sustainability. pp. 11-27. Springer, Singapore. https://doi.org/10.1007/978-981-10-7551-3_2

Mishra, A., Tripathi, B.D. and A.K. Rai (2016). Packed-bed column biosorption of chromium (VI) and nickel (II) onto Fenton modified *Hydrilla verticillata* dried biomass. Ecotoxicology and *Environmental Safety*, **132:** 420-428.

Murphy, J.N. and F.M. Kerton (2017). Characterization and utilization of waste streams from mollusc aquaculture and fishing industries, *In:* Kerton, F.M. and N. Yan (eds.). Fuels, Chemicals and Materials from the Oceans and Aquatic Sources, **58:** 189-225. John Wiley & Sons Ltd.

Naushad, M., Ahamad, T., AlOthman, Z.A. and H. Ala'a (2019). Green and eco-friendly nanocomposite for the removal of toxic Hg (II) metal ion from aqueous environment: Adsorption kinetics & isotherm modelling. *Journal of Molecular Liquids*, **279:** 1-8.

Nithya, K., Sathish, A. and P.S. Kumar (2020). Packed bed column optimization and modeling studies for removal of chromium ions using chemically modified *Lantana camara* adsorbent. Journal of Water Process Engineering, **33:** 101069.

Nithya, K., Sathish, A. and P. Senthil Kumar (2021). Magnetite encapsulated alginates tailored material for the sustainable treatment of electroplating industrial wastewater: Column dynamics and mass transfer studies. *Clean Technologies and Environmental Policy*, **23(1):** 89-102.

Núñez, D., Serrano, J.A., Mancisidor, A., Elgueta, E., Varaprasad, K., Oyarzún, P., et al. (2019). Heavy metal removal from aqueous systems using hydroxyapatite nanocrystals derived from clam shells. *RSC Advances*, **9(40):** 22883-22890.

Papadimitriou, C.A., Krey, G., Stamatis, N. and A. Kallianiotis (2017). The use of waste mussel shells for the adsorption of dyes and heavy metals. *Journal of Chemical Technology & Biotechnolog*y, **92(8):** 1943-1947.

Qu, J., Song, T., Liang, J., Bai, X., Li, Y., Wei, Y. and Y.U. Jin (2019). Adsorption of lead (II) from aqueous solution by modified Auricularia matrix waste: A fixed-bed column study. *Ecotoxicology and Environmental Safety*, **169:** 722-729.

Qu, T., Yao, X., Owens, G., Gao, L. and H. Zhang (2022). A sustainable natural clam shell derived photocatalyst for the effective adsorption and photodegradation of organic dyes. *Scientific Reports*, **12(1):** 1-14.

Rangabhashiyam, S., Anu, N. and N. Selvaraju (2013). Sequestration of dye from textile industry wastewater using agricultural waste products as adsorbents. *Journal of Environmental Chemical Engineering*, **1(4):** 629-641.

Santhosh, S. and S.B. Prabu (2012). Synthesis and characterisation of nanocrystalline hydroxyapatite from sea shells. *International Journal of Biomedical Nanoscience and Nanotechnology*, **2(3-4):** 276-283.

Singh, D.K., Kumar, V., Mohan, S., Bano, D. and S.H. Hasan (2017). Breakthrough curve modeling of graphene oxide aerogel packed fixed bed column for the removal of Cr (VI) from water. *Journal of Water Process Engineering*, **18:** 150-158.

Sugashini, S. and K.M.M.S. Begum (2014). Performance of Fe-loaded chitosan carbonized rice husk beads (Fe-CCRB) for continuous adsorption of metal ions from industrial effluents. *Environmental Progress & Sustainable Energy*, **33(4):** 1125-1138.

Sumesh, E., Bootharaju, M.S. and T. Pradeep (2011). A practical silver nanoparticle-based adsorbent for the removal of Hg^{2+} from water. *Journal of Hazardous Materials*, **189(1-2):** 450-457.

Suresh, P., Sharmila, N. and V.K. Ch (2019). ICP-OES determination of trace metals in groundwater of Proddatur area, YSR Kadapa dist., AP-India. *Caribbean Journal of Sciences and Technology (CJST)*, **7(1):** 001-007.

Tsai, C.Y., Liu, C.W., Hsi, H.C., Lin, K.S., Lin, Y.W. and L.C. Lai (2019). Synthesis of Ag-modified TiO_2 nanotube and its application in photocatalytic degradation of dyes and elemental mercury. *Journal of Chemical Technology & Biotechnology*, **94(10):** 3251-3262.

Urgun-Demirtas, M., Benda, P.L., Gillenwater, P.S., Negri, M.C., Xiong, H. and S.W. Snyder (2012). Achieving very low mercury levels in refinery wastewater by membrane filtration. *Journal of Hazardous Materials*, **215:** 98-107.

Vishalia, S., Mullaib, P. and R. Karthikeyanc (2019). Breakthrough studies and mass transfer studies on the decolorization of paint industry wastewater using encapsulated beads of *Cactus opuntia* (*Ficus-indica*). *Desalination and Water Treatment*, **177:** 89-101.